International Journal of
MATERIALS RESEARCH

Zeitschrift für METALLKUNDE

Original Contributions

Haibin Tang, Haiding Guo

Jiangsu Province Key Laboratory of Aerospace Power System, Collaborative Innovation Center for Advanced Aero-Engine, Nanjing University of Aeronautics and Astronautics, Nanjing, China

Effect of grain defects on the mechanical behavior of nickel-based single crystal superalloy

In this paper, a single crystal (SC) partition model, consisting of primary grains and grain defects, is proposed to simulate the weakening effect of grain defects generated at geometric discontinuities of SC materials. The plastic deformation of SC superalloy is described with the modified yield criterion, associated flow rule and hardening law. Then a bicrystal model containing only one group of misoriented grains under uniaxial loading is constructed and analyzed in the commercial finite element software ABAQUS. The simulation results indicate that the yield strength and elastic modulus of misoriented grains, which are determined by the crystallographic orientation, have a significant effect on the stress distribution of the bicrystal model. A critical stress, which is calculated by the stress state at critical regions, is proposed to evaluate the local stress rise at the sub-boundary of primary and misoriented grains.

Keywords: Nickel-based single crystal superalloy; Grain defects; Single crystal partition model; Local stress rise; Critical stress

1. Introduction

In the modern aviation industry, advanced materials applied in the hot section are a critical issue to ensure the economic and reliable performance of aeroengines. Nickel-based single crystal (SC) superalloys have been increasingly used to manufacture turbine blades in high performance aircraft and rocket engines [1–5]. Compared with polycrystalline materials or directionally solidified alloys, SC superalloys have better mechanical properties at elevated temperature due to the absence of weak grain boundaries.

SC superalloy is a two-phase material made of intermetallic γ' precipitates and face-centered cubic γ matrix, which results in high material anisotropy [6–10]. In the last several decades two main approaches have been proposed to describe the mechanical properties of SC superalloy. The first approach is based on the crystallographic slip theory [6, 11–13]. The texture changes inside the material can be tracked and therefore the texture-induced anisotropy can be evaluated accordingly. However, the requirement of enormous computational power and time limits its usage in engineering practice. An alternative approach is through use of a phenomenological yield criterion [14–17], which is also paid high attention to in theoretical research and practical applications, due to simplicity and convenience.

As for grain defects' effects on mechanical properties, only limited research work can be found. However, during the manufacture of complex structures such as turbine blades, grain defects would be generated in the SC superalloy casting by directional solidification [18–24]. It has been shown that thermal condition and mold geometry have a significant impact on the formation of grain defects [25, 26]. The disordered temperature distribution at geometric discontinuities, e. g. blade shrouds, turbine blade platforms and turbine blade rabbets, can result in distortions in the crystal lattice [27]. Usually, grain defects are observed at critical locations along with complex stress states, and the mechanical and fatigue characteristics of SC superalloy would be greatly influenced by grain defects [27, 28], so

the effect of grain defects on SC complex structures should be considered.

So far, the basic material properties of SC superalloy containing grain defects have been studied experimentally [27, 29–32]. However, there is still a lack of numerical modeling and theoretical analysis of grain defects' effects on SC materials. In this paper, an SC partition model is constructed, and the effect of misoriented grains on the mechanical behaviors of SC materials is further investigated by the bicrystal model through finite element analysis.

2. The SC partition model

2.1. Theoretical basis of SC partition model

X-ray topography of SC material Rene N5 containing grain defects was given by Napolitano and Schaefer [26], and major grain defects were categorized as low-angle boundaries, high-angle boundaries and spurious grains, shown in Fig. 1a. The crystal morphology of SC material AM3 containing grain defects was studied by Zhao et al. [33]. The result showed that grain defects can be divided into several groups, in which the primary stems were aligned into rows, and high-angle boundaries were observed, as shown in Fig. 1b. The casting microstructure of SC material DD6 containing grain defects was investigated by Shi et al. [34], and the misoriented grains along [111] were also observed, as given in Fig. 1c.

In this paper, these typical grain defects are analyzed, including low-angle boundaries, high-angle boundaries and spurious grains (stray grains).

Based on X-ray topography or predictions, the microstructure and locations of grain defects are obtained, and then the SC structure can be divided into several partitions. Given a single partition, for the case with primary or misoriented grains, it can be still modeled as SC material along the corresponding direction, and for the case with spurious grains, isotropic model can be used instead.

2.2. The constitutive model for SC superalloy

At the continuum scale, for a multi-axial stress space, plastic deformation of SC superalloy can be fully described with the combination of a yield surface, a flow rule and a hardening law. It is necessary to rebuild suitable constitutive relationships for SC superalloy. On this basis, a coordinate transformation matrix is used, as the finite element calculation for different partitions should be carried out in their principal material coordinate system, respectively.

2.2.1. The modified yield criterion for SC superalloy

The shape of the yield surface of SC materials is dictated by the requirements of:

1. Pressure-independence.
2. Normal–shear coupling effect [16, 17, 35, 36].
3. Tension–compression asymmetry [37–41].
4. Equal yield strength along three principal material directions [17].

On the basis of the Hill 1948 yield criterion, a modified yield criterion of SC material is proposed. When x, y and z

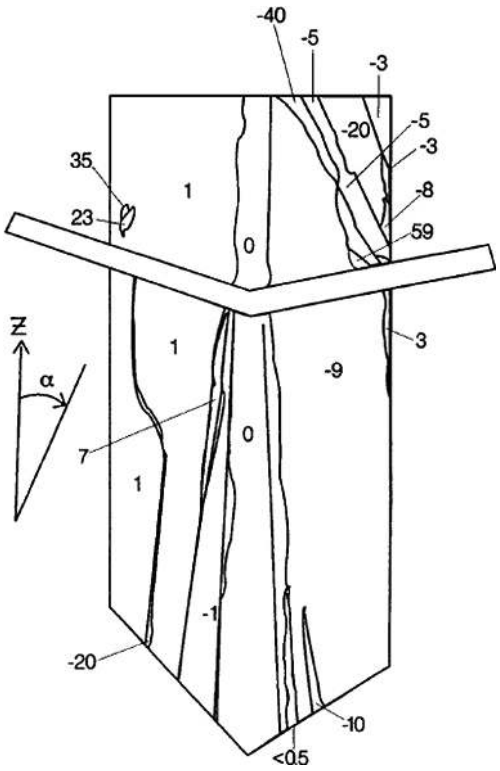

(a)

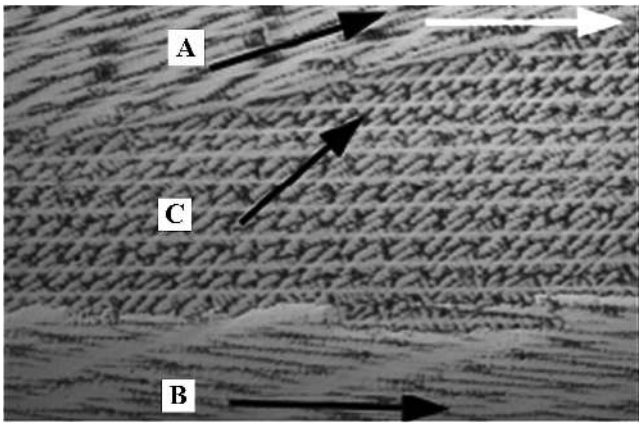

(b)

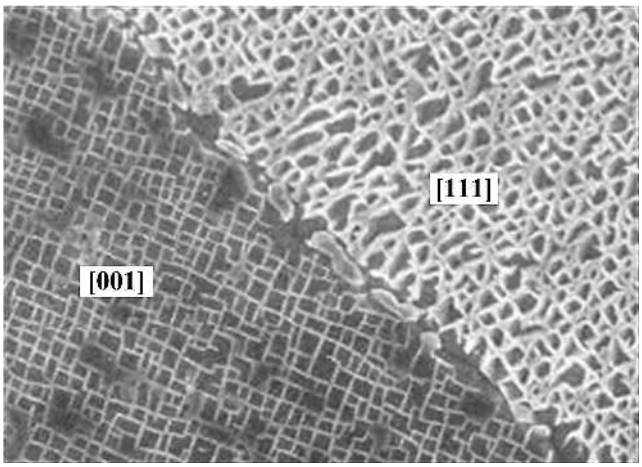

(c)

Fig. 1. Microstructure of SC superalloys containing grain defects: (a) SC superalloy Rene N5 from Ref. [26], (b) SC superalloy AM3 from Ref. [33], and (c) SC superalloy DD6 from Ref. [34].

axes for SC superalloy coincide with [100], [010] and [001] direction, it has the following form:

$$(J_2^0)^{\frac{3}{2}} - J_3^0 = Y^3 \tag{1}$$

$$J_2^0 = [(P_1 + P_2)^2 + P_6]^{\frac{1}{2}}$$

$$P_1 = \frac{A}{6}[(S_x - S_y)^2 + (S_y - S_z)^2 + (S_z - S_x)^2];$$

$$P_2 = B(S_{xy}^2 + S_{yz}^2 + S_{zx}^2);$$

$$P_6 = C([(S_z - S_y)^2 + (S_z - S_x)^2]S_{xy}^2 + [(S_x - S_z)^2 + (S_x - S_y)^2]S_{yz}^2 + [(S_y - S_x)^2 + (S_y - S_z)^2]S_{zx}^2);$$

$$J_3^0 = \frac{a}{3}(S_x^3 + S_y^3 + S_z^3) + 2bS_{xy}S_{yz}S_{zx} - \frac{c}{3}(S_zS_{xy}^2 + S_xS_{yz}^2 + S_yS_{zx}^2)$$

where A, B, C, a, b, c are material parameters. Y is the uniaxial yield strength along [001] direction. It is generally agreed that the yield behavior of SC superalloy is influenced by the normal–shear coupling effect [16, 17, 35, 36] and the tension–compression asymmetry [37–41]. The material parameter C is independent, which can be used to describe the coupling effect, and the material parameters a, b, c are also independent, which are exactly used to describe the asymmetry. By comparison, the Hill 1948 yield criterion is not suited to describing the yield surface of SC superalloy accurately.

While the compression is not considered in the analysis of yield behavior, the asymmetry has little influence on experimental and theoretical yield loci, then, a, b, $c = 0$. Subsequently, the modified yield criterion of SC superalloy reduces to Eq. (2):

$$Y^2 = [(P_1 + P_2)^2 + P_6]^{\frac{1}{2}} \tag{2}$$

According to the tensile experiments of SC superalloy DD3 provided by Ding [17] (detailed in Table 1), the independent parameters involved in Eq. (2) (A, B and C) can be calculated from the tensile yield strength of DD3 along [001], [011] and [111] directions, and the results can be used to predict the tensile yield strength along [112], which are shown in Table 1. For the sake of comparison, the predictions given by the Hill 1948 yield criterion are also listed in Table 2.

It should be mentioned that the independent parameters in the Hill 1948 yield criterion for DD3 can be calculated from the yield strength of [001] and [111] directions. Thus the predictions along [011] direction can also be used to validate the Hill 1948 yield criterion. At the temperatures 950 °C and 850 °C, the relative error is just 4.6 % and 0.1 %, respectively. However, it rises up to 9.9 % and 14.1 % at 760 °C and 680 °C, respectively.

The dislocation configuration and the type of activated slip systems are influenced by the thermal activation. At elevated temperature, the normal–shear coupling is reduced and in some cases eliminated. Thus, the predictions given by these two yield criteria fit well with the experiments. However, for the Hill 1948 yield criterion, deviations occur at 760 °C and 680 °C, which are ascribed to the normal–shear coupling effect. Compared with it, the modified yield criterion is better suited to describing the yield surface of SC superalloy.

2.2.2. Elastic–plastic matrix of SC superalloy

The associated flow rule is employed to build up the relationship between plastic strain increment and deviatoric stress tensor for SC superalloy. When plastic deformation is further increased, the variation of yield surface is determined by the hardening law. The unique evolution of SC superalloy yield surface is neither isotropic nor kinematic [42]. Actually, both isotropic and kinematic hardening variables should be considered to describe the cyclic behavior [14, 43], and the corresponding equations are listed in Zhao and Tong [14].

During the analysis of monotonic behavior for SC superalloy, the isotropic hardening law can be used for describing the plastic deformation of SC superalloy, which has little influence on the simulation results. Then the elastic–plastic matrix can be derived as [44]:

$$[C]_{\mathrm{ep}} = [C]_{\mathrm{e}} - \frac{[C]_{\mathrm{e}}\left\{\frac{\partial\bar{\sigma}}{\partial\sigma}\right\}\left\{\frac{\partial\bar{\sigma}}{\partial\sigma}\right\}^T[C]_{\mathrm{e}}}{H' + \left\{\frac{\partial\bar{\sigma}}{\partial\sigma}\right\}^T[C]_{\mathrm{e}}\left\{\frac{\partial\bar{\sigma}}{\partial\sigma}\right\}} \tag{3}$$

where $[C]_{\mathrm{e}}$ is the elastic stiffness matrix. H' is the slope of the stress–plastic strain curve. $\bar{\sigma}$ is the SC equivalent stress which is written as,

$$\bar{\sigma} = [(J_2^0)^{\frac{3}{2}} - J_3^0]^{\frac{1}{3}} \tag{4}$$

2.3. Coordinate transformation for different partitions

Misoriented grains in each partition can be divided into two kinds: tilt and twist misoriented grains, which are formed by edge and screw dislocation, respectively [29]. The misorientation α, which has been adopted in the definition of grain defects [22, 29–32], is not able to distinguish the mis-

Table 1. Experimental tensile yield strength of DD3 along different directions.

Temperature (°C)	950	850	760	680
[001]	525	870	915	943
[011]	490	840	899	896
[111]	510	830	1030	1085
[112]	530	809	880	–

Table 2. Theoretical tensile yield strength of DD3 along [112] direction.

Temperature (°C)	950	850	760
Modified criterion	500	840	937
Relative error (%)	5.7	3.8	6.4
Hill's criterion	514	839	997
Relative error (%)	3.2	3.6	11.8

oriented grains in different crystallographic orientations or twisted to different angles. Thus, [*hklθ*] is introduced in this paper, where [*hkl*] is the tilt orientation of misoriented grains, and θ is angle of twist. Since the finite element calculation of misoriented grains should be carried out in their principal material coordinate system, the transformation between global and principal material coordinate system is needed. Figure 2 shows the relationship between the global coordinate system $OX_MY_MZ_M$, transitional coordinate system $OX_GY_TZ_T$ and principal material coordinate system $OX_GY_GZ_G$. The transformation of $OX_MY_MZ_M$ and $OX_GY_TZ_T$ is suited for the tilt misoriented grains irrespective of the twisting. Here, the subscripts M, T and G refer to material, transitional and global, respectively.

$\{\sigma\}_G$, $\{\varepsilon\}_G$, and $[C]_G$ denote to the stress tensor, strain tensor, stiffness matrix in the global coordinate system. $\{\sigma\}_M$, $\{\varepsilon\}_M$ and $[C]_M$ denote to the stress tensor, strain tensor, stiffness matrix in the principal material coordinate system. Then it follows that,

$$\begin{aligned} \{\sigma\}_M &= [T_\sigma]\{\sigma\}_G \\ \{\varepsilon\}_M &= [T_\varepsilon]\{\varepsilon\}_G \\ [C]_G &= [T_\sigma]^{-1}[C]_M[T_\varepsilon] \end{aligned} \tag{5}$$

3. The bicrystal model

3.1. The simplified mathematical model

The SC partition model will be simplified in order to discuss the effect of misoriented grains on the stress distribution of SC structures thoroughly. Then, a bicrystal model containing only one group of misoriented grains is proposed, as detailed in Fig. 3. The left and right parts of the bicrystal model represent the primary and misoriented grains, respectively. The bicrystal model is fixed at one end and a concentrated load applied at other end horizontally. β is the angle between the interface of sub-boundary and the orientation of primary grains, which is different from α. A wide range of β can be expected in the real SC structures.

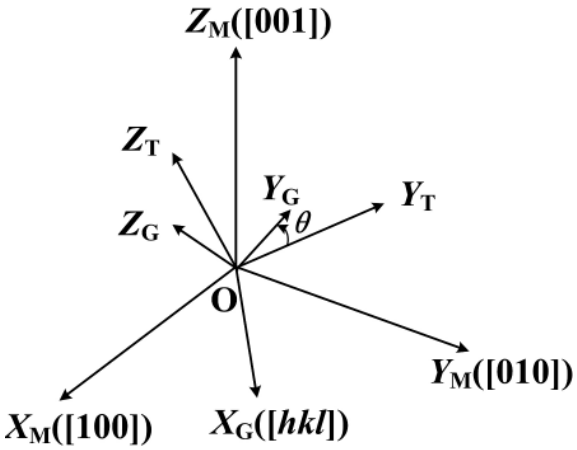

Fig. 2. Transformation of coordinate system for different partitions in SC structures.

3.2. Material parameters for DD3 bicrystal model

According to the bicrystal model as illustrated in Fig. 3, an 3D model is built in ABAQUS, the model dimension is 60 mm × 10 mm × 4 mm, and $\beta = 30°$. The primary grains are along [001], and the misoriented grains are labeled as from QX1 to QX9 for different crystallographic orientations. The non-linear large deflection algorithm is enabled through the finite element analysis to accurately capture the local plastic deformation.

Note that the compression is not included in numerical simulation, and then Eq. (2) can be served as the yield criterion of SC superalloy. Some essential material parameters for DD3 bicrystal model (680 °C) are provided by Ding [17], as listed in Table 3. Here, $\phi'_{[001]}$ is the plastic modulus of DD3 along [001] direction. $\sigma_{y[001]}$, $\sigma_{y[011]}$ and $\sigma_{y[111]}$ are the tensile yield strengths of DD3 along [001], [011] and [111] directions respectively. For quantitative analysis, the basic material properties of misoriented grains are calculated by the proposed SC constitutive model, as detailed in Table 4. Among them, σ_{ym}, E_m and ϕ_m are the yield strength, elastic modulus and plastic modulus of DD3 along specific directions, respectively.

4. Influence analysis based on the bicrystal model

4.1. The critical stress in the bicrystal model

The SC equivalent stress, as defined in Eq. (4), is introduced to evaluate the stress distribution of SC structures. According to the finite element analysis results, non-uniform stress distribution and critical region (marked as A or B) are always observed under axial tensile load. The SC equivalent stress contours under different loads are illustrated in Fig. 4a–d, which are obtained from two typical configurations. Here $\bar{f}$ denotes to the nominal surface force.

To evaluate the local stress rise near the sub-boundary, an SC critical stress σ_d is proposed, which is the SC equivalent stress at the critical region (A or B). Figure 5a presents

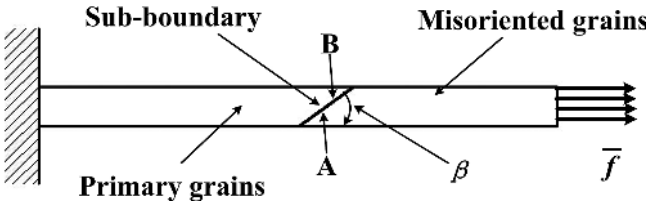

Fig. 3. The bicrystal model.

Table 3. Tensile test results of DD3 along [001], [011] and [111] directions (680 °C).

G (GPa)	μ	$E_{[001]}$ (GPa)	$\phi'_{[001]}$ (GPa)	$\sigma_{y[001]}$ (MPa)	$\sigma_{y[011]}$ (MPa)	$\sigma_{y[111]}$ (MPa)
113	0.322	129.7	1.328	943	896	1085

the relationship between σ_d and $\bar{f}$ for the DD3 bicrystal model containing misoriented grains QX5; Figure 5b shows the relationship between σ_d and $\bar{f}$ for the DD3 bicrystal model containing different misoriented grains (partly). For the sake of comparison, the mechanical behavior of only primary grains is also given in Fig. 5b. The simulation results indicate that the mechanical behavior of SC structure is distinctly influenced by the misoriented grains. According to Fig. 5a and b, the loading process of the bicrystal model can be divided into three stages:

1. Elastic stage.
2. Local elastic–plastic stage I.
3. Larger elastic–plastic stage II.

In the elastic stage, the stress state near the sub-boundary is determined by the elastic modulus of primary grains, E_0, and the elastic modulus of misoriented grains, E_m. Local high stress is observed near region A, as detailed in Fig. 4a and b. The local stress rise is a little unremarkable for a low-angle boundary ($\alpha \leq 6°$), while it is much pronounced for a high-angle boundary ($\alpha \geq 10°$). As the load increases, the material at region A will yield firstly.

In the local elastic–plastic stage I, the local stress rise is still located at region A. It could be shown that, with the increase in load, the local stress rise tends to be less distinct and more misoriented grains reach the initial yield stress.

In the larger elastic–plastic stage II, the variation of σ_d is mainly determined by the yield strength of primary grains, σ_{y0}, and the yield strength of misoriented grains, σ_{ym} While σ_{ym} is smaller than σ_{y0} (e. g. QX5), the critical region will be transferred from A to B, as shown in Fig. 4c. The lower σ_{ym} is, the smaller load the bicrystal structure can sustain. With the increase in load, more primary grains reach the initial yield stress.

Table 4. Basic material properties of DD3 along specific directions (680 °C).

ID	Misoriented grains [$hkl\theta$]				α (°)	σ_{ym} (MPa)	E_m (GPa)	ϕ'_m (GPa)
	h	k	l	θ				
QX1	0	0.105	1	0	6	935.50	131.83	1.308
QX2	0	0.177	1	0	10	924.50	135.65	1.278
QX3	0	0.268	1	0	15	909.50	143.08	1.237
QX4	0.189	0.189	1	0	15	911.81	143.35	1.244
QX5	0	0.577	1	0	30	888.31	180.34	1.183
QX6	0.408	0.408	1	0	30	919.20	186.33	1.267
QX7	0	1	1	0	45	895.80	207.21	1.204
QX8	0.707	0.707	1	0	45	1031.18	243.60	1.594
QX9	1	1	1	0	54.74	1084.80	258.75	1.764

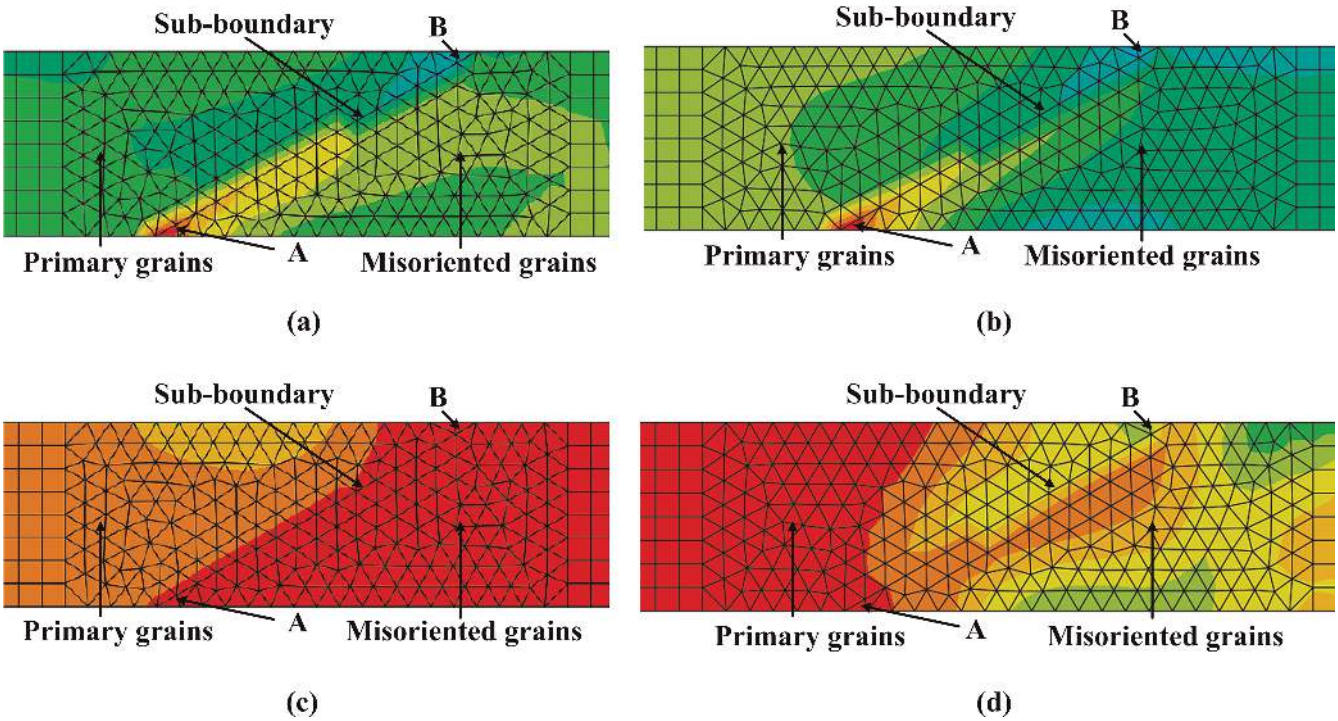

Fig. 4. SC equivalent stress contour of the DD3 bicrystal model: (a) $\bar{f} = 600$ MPa, containing QX5, (b) $\bar{f} = 600$ MPa, containing QX9, (c) $\bar{f} = 892$ MPa, containing QX5, and (d) $\bar{f} = 950$ MPa, containing QX9.

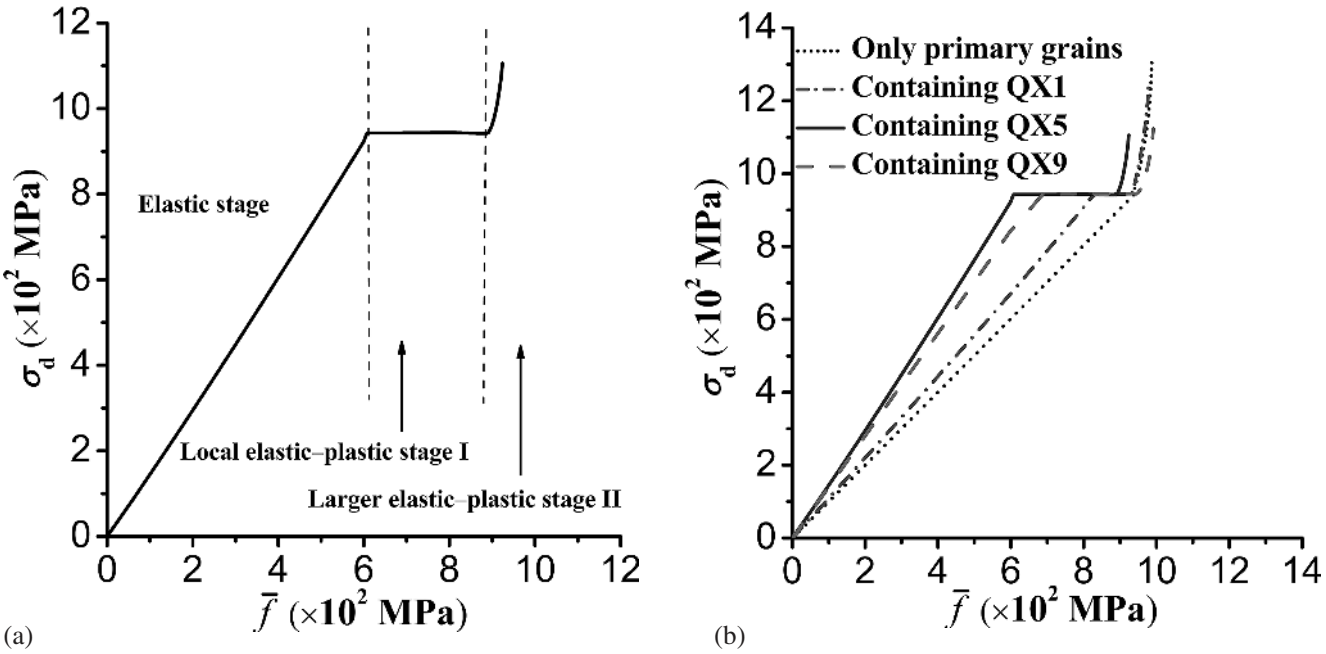

Fig. 5. Relationship between σ_d and $\bar{f}$ for the DD3 bicrystal model: (a) containing QX5, and (b) containing different misoriented grains.

While σ_{ym} is larger than σ_{y0} (e.g. QX9), Region A will always be the most critical location, as shown in Fig. 4d. The maximum load which the bicrystal structure can sustain is nearly the same. It should be noted that local stress rise location around sub-boundary is still a critical region in consideration of the fragility of sub-boundary in the larger elastic–plastic stage II, while the maximum equivalent stress of the grains with lower yield strength will increase rapidly due to necking.

4.2. Evolution equation of the critical stress

The critical stress observed near the sub-boundary has been analyzed in Section 4.1, and so the corresponding evolution equation of critical stress can be constructed.

4.2.1. Elastic stage

There is a significant linear correlation between σ_d and $\bar{f}$, as shown in Fig. 5b. As the slope of the linear relationship is influenced by E_0, E_m, σ_{y0} and σ_{ym}, it can be calculated by regression analysis. Thus, the evolution equation of σ_d in the elastic stage is given as:

$$\sigma_d = \left[\left(\frac{E_m - E_0}{E_m}\right)^{0.546} + 1\right]\frac{\sigma_{y0}}{\sigma_{ym}}\bar{f} \tag{6}$$

Since $\sigma_d \le \sigma_{y0}$, the range of load is obtained as:

$$0 \le \bar{f} \le \frac{\sigma_{y0}}{\left[\left(\frac{E_m - E_0}{E_m}\right)^{0.546} + 1\right]\frac{\sigma_{y0}}{\sigma_{ym}}} \tag{7}$$

4.2.2. Local elastic–plastic stage I

The range of load is expressed as:

$$\frac{\sigma_{y0}}{\left[\left(\frac{E_m - E_0}{E_m}\right)^{0.546} + 1\right]\frac{\sigma_{y0}}{\sigma_{ym}}} \le \bar{f} \le \sigma_c \tag{8}$$

where σ_c is very close to the smaller of σ_{y0} and σ_{ym}. As shown in Fig. 5b, the increase in applied load has little influence on σ_d. Thus, the evolution equation of σ_d in this stage has the following form:

$$\sigma_d = \sigma_{y0} \tag{9}$$

4.2.3. Larger elastic–plastic stage II

The range of load is written as:

$$\bar{f} \ge \sigma_c \tag{10}$$

In the bicrystal model, the difference in the magnitudes of σ_{y0} and σ_{ym} will result in a different critical region, and σ_d will also change differently. Figure 6a and b presents the relationship between σ_d and $\bar{f}$ for the DD3 bicrystal model containing different misoriented grains in the larger elastic–plastic stage II.

While $\sigma_{ym} < \sigma_{y0}$, the evolution equation of σ_d is mathematically represented as follows:

$$\sigma_d = 1.52(\bar{f} - \sigma_c)^{1.38} + \sigma_{y0} \tag{11}$$

While $\sigma_{ym} > \sigma_{y0}$, the evolution equation of σ_d in this stage has the following expression:

$$\sigma_d = 0.14(\bar{f} - \sigma_c)^{1.88} + \sigma_{y0} \tag{12}$$

Finally, the evolution equation of σ_d can be summarized as follows (see Eq. (13) on the bottom of this page).

5. Discussion

(1) As analyzed above, the stress distribution of the bicrystal model is influenced by crystallographic orientation. In contrast, the angle of twist, θ, has little impact on mechanical analysis for the bicrystal model, which is attributed to the specific loading condition in this model. The variation of θ would result in different mechanical behavior in transverse directions, but the corresponding stress components are much smaller and just induced by the heterogeneous structure.

By comparison, the effect of angle β should also be considered in the mechanical analysis for bicrystal model. The same 3D model except for β is built in ABAQUS. The primary grains are along [001], and the misoriented grains are QX5. β equals to 20°, 30° and 45°, respectively. Figure 7 presents the relationship between σ_d and $\bar{f}$ for the DD3 bicrystal model with different β. The result shows that the local stress rise will be more distinct and the loading process will be longer in the elastic stage, with decrease in β. However, β has little influence on mechanical behavior of SC material containing misoriented grains in the local elastic–plastic stage I and larger elastic–plastic stage II.

(2) The SC material containing only one group of misoriented grains is an ordinary condition. Actually, as shown in Fig. 1a, quite a few SC materials contain several groups of misoriented grains. Then, the real SC structures can be analyzed with the proposed SC partition model. A representative sample containing three groups of misoriented grains, which is more similar to the real SC structure, is built in ABAQUS, as detailed in Fig. 8. The SC equivalent stress distribution of the sample under the axial tensile loading is shown in Fig. 9. The local high stress is observed near the sub-boundary of different partitions. The numerical simulation shows that the stress distribution and critical stress are influenced by the crystallographic orientations and locations of partitions.

(3) It is generally agreed that grain defects would act as favorable locations for crack initiation for SC structures containing grain defects [25, 28]. Yan et al. [27] carried out comparative low cycle fatigue experiments of directionally solidified materials. Fatigue rupture was observed at the grain defects regions for specimens containing grain defects. In particular, the life cycles of specimens containing

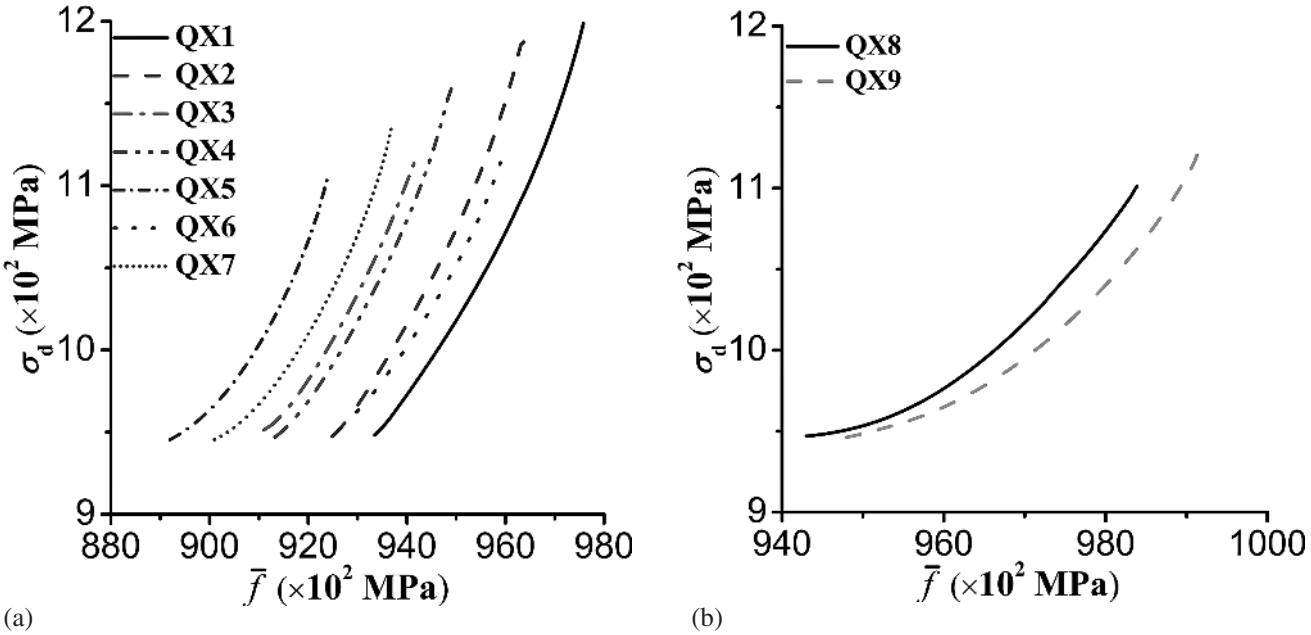

Fig. 6. Relationship between σ_d and $\bar{f}$ in the larger elastic–plastic stage II: (a) $\sigma_{ym} < \sigma_{y0}$, and (b) $\sigma_{ym} > \sigma_{y0}$.

$$\sigma_d = \begin{cases} \left[\left(\dfrac{E_m - E_0}{E_m}\right)^{0.546} + 1\right]\dfrac{\sigma_{y0}}{\sigma_{ym}}\bar{f}, & 0 \le \bar{f} \le \dfrac{\sigma_{y0}}{\left[\left(\dfrac{E_m - E_0}{E_m}\right)^{0.546} + 1\right]\dfrac{\sigma_{y0}}{\sigma_{ym}}} \\ \sigma_{y0}, & \dfrac{\sigma_{y0}}{\left[\left(\dfrac{E_m - E_0}{E_m}\right)^{0.546} + 1\right]\dfrac{\sigma_{y0}}{\sigma_{ym}}} \le \bar{f} \le \sigma_c \\ 1.52(\bar{f} - \sigma_c)^{1.38} + \sigma_{y0}, & \bar{f} \ge \sigma_c \text{ and } \sigma_{ym} < \sigma_{y0} \\ 0.14(\bar{f} - \sigma_c)^{1.88} + \sigma_{y0}, & \bar{f} \ge \sigma_c \text{ and } \sigma_{ym} > \sigma_{y0} \end{cases} \quad (13)$$

grain defects were much less than normal specimens. Moreover, grain defects would generate during solidification of SC superalloy welds. The crack nucleation and propagation were also always observed at these grain defect regions [45, 46].

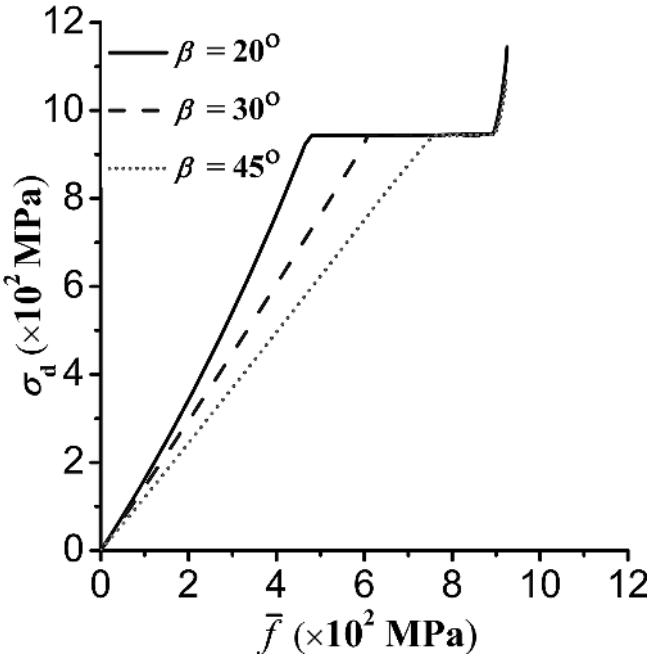

Fig. 7. Relationship between σ_d and $\bar{f}$ for the bicrystal model with different β.

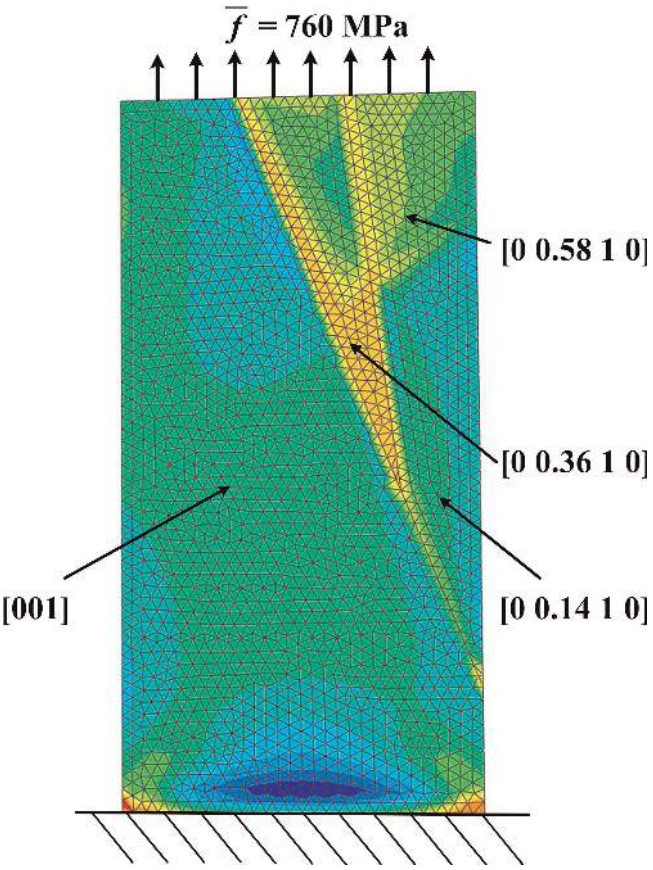

Fig. 9. SC equivalent stress contour of the representative sample.

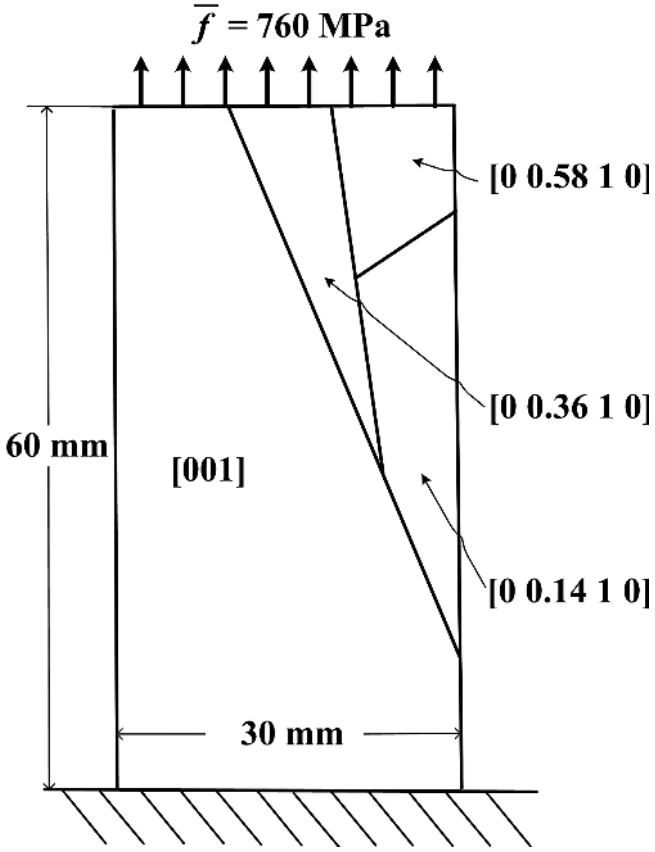

Fig. 8. The geometry of the representative sample.

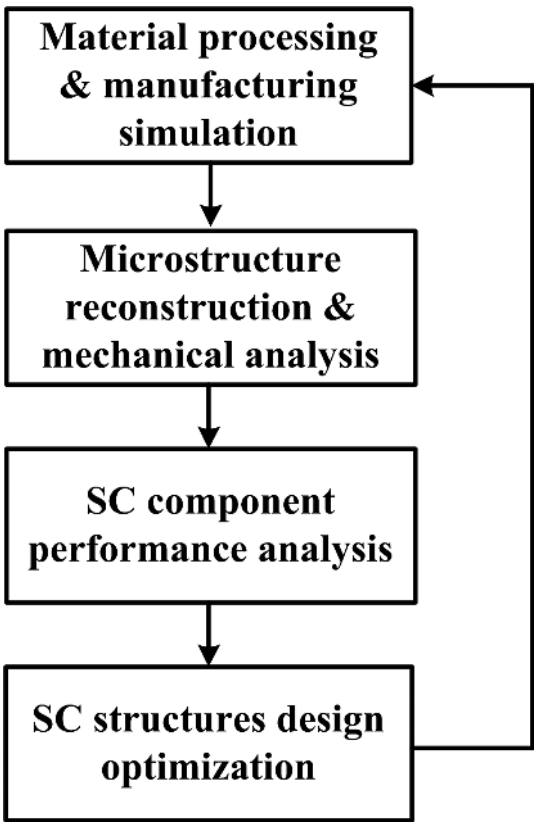

Fig. 10. Process integration & design optimization tool for SC structures.

According to numerical simulation, for the SC structures containing grain defects, the critical region is always observed near the sub-boundary, which coincides with these experiments mentioned above. Hence, the effect of grain defects should be considered in the analysis of the mechanical behavior and fatigue characteristics of SC complex structures.

(4) On the basis of SC manufacturing simulation and SC partition model, an integrated workflow of computational models will be established in the near future to enable the manufacturing optimization, as illustrated in Fig. 10. Further work will involve applying the mechanical analysis to life predictions of SC structures.?A3B2 tpb 4dd?>

6. Conclusions

1. A new SC (single crystal) partition model, consisting of primary grains and grain defects, is proposed to simulate the weakening effect of grain defects generated at geometric discontinuities of SC structures.
2. A modified SC yield criterion is constructed, which can describe the yield characteristics of SC materials namely the normal–shear coupling and tension–compression asymmetry.
3. A bicrystal model containing only one group of misoriented grains under uniaxial loading is built to analyze the effect of misoriented grains on the stress distribution of SC superalloy thoroughly.
4. The yield strength and elastic modulus of misoriented grains, which are determined by the crystallographic orientation, have a significant effect on the stress distribution of the bicrystal model.
5. The evolution equation of critical stress, which is the SC equivalent stress at the critical region, is constructed to evaluate the effect of misoriented grains on the stress distribution.

This research is supported by Jiangsu Province Key Laboratory of Aerospace Power System. The authors are indebted to S.H. Yang and Dr. L. Huang for the detailed discussion of this work.

References

[1] O. Okazaki, M. Sakaguchi: Int. J. Fatigue 30 (2008) 318–323. DOI:10.1016/j.ijfatigue.2007.01.044
[2] D. Leidermark, J. Moverare, K. Simonsson, S. Sjostrom: Int. J. Fatigue 33 (2011) 1351–1359. DOI:10.1016/j.ijfatigue.2011.05.009
[3] J. Durocher, J.R. Cahoon, N.L. Richards: Mater. Sci. Technol. 29 (2013) 534–541. DOI:10.1179/1743284712Y.0000000186
[4] L. Remy, M. Geuffrard, A. Alam, A. Koster, E. Fleury: Int. J. Fatigue 57 (2013) 37–49. DOI:10.1016/j.ijfatigue.2012.10.013
[5] P. Li, Q.Q. Li, T. Jin, Y.Z. Zhou, J.G. Li, X.F. Sun, Z.F. Zhang: Int. J. Fatigue 63 (2014) 137–144. DOI:10.1016/j.ijfatigue.2014.01.018
[6] B. Fedelich: Int. J. Plast. 18 (2002) 1–49. DOI:10.1016/S0749-6419(00)00045-0
[7] R.A. Naik, D.P. Deluca, D.M. Shah: J. Eng. Gas Turbines Power 126 (2004) 391–400. DOI:10.1115/1.1690768
[8] D. Leidermark, J. Moverare, K. Simonsson, S. Sjostrom, S. Johansson: Procedia Eng. 2 (2010) 1067–1075. DOI:10.1016/j.proeng.2010.03.115
[9] M. Segersall, D. Leidermark, J.J. Moverare: Mater. Sci. Eng. A 623 (2015) 68–77. DOI:10.1016/j.msea.2014.11.026
[10] J.B. le Graverend, J. Cormier, F. Gallerneau, S. Kruch, J. Mendez: Int. J. Fatigue 91 (2016) 257–263. DOI:10.1016/j.ijfatigue.2016.06.018
[11] J.B. le Graverend, J. Cormier, F. Gallerneau, P. Villechaise, S. Kruch, J. Mendez: Int. J. Plast. 59 (2014) 55–83. DOI:10.1016/j.ijplas.2014.03.004
[12] J. Cormier, G. Cailletaud: Mater. Sci. Eng. A 527 (2010) 6300–6312. DOI:10.1016/j.msea.2010.06.023
[13] E.P. Busso, F.T. Meissonnier, N.P. O'Dowd: J. Mech. Phys. Solids 48 (2000) 2333–2361. DOI:10.1016/S0022-5096(00)00006-5
[14] L.G. Zhao, J. Tong: J. Mech. Phys. Solids 56 (2008) 3363–3378. DOI:10.1016/j.jmps.2008.09.006
[15] L.G. Zhao, J. Tong: J. Mater. Sci. 40 (2005) 1229–1235. DOI:10.1007/s10853-005-6941-1
[16] L.H. Yang, G.P. Zou, Q. Jia: Key Eng. Mater. 525–526 (2012) 341–344. DOI:10.4028/www.scientific.net/KEM.525-526.341
[17] Z.P. Ding: PhD thesis, Study on multiaxial low cycle fatigue damage of single crystal nickel-based superalloy, Central South University, China (2005).
[18] N. D'Souza, P.A. Jennings, X.L. Yang, H.B. Dong, P.D. Lee, M. Mclean: Metall. Mater. Trans. B. 36 (2005) 657–666. DOI:10.1007/s11663-005-0056-6
[19] M. Newell, K. Devendra, P.A. Jennings, N. D'Souza: Mater. Sci. Eng. A 412 (2005) 307–315. DOI:10.1016/j.msea.2005.09.030
[20] T.M. Pollock, S. Tin: J. Propul. Power. 22 (2006) 361–374. DOI:10.2514/1.18239
[21] T.D. Anderson, J.N. DuPont, T. DebRov: Acta Mater. 58 (2010) 1441–1454. DOI:10.1016/j.actamat.2009.10.051
[22] Y.Z. Zhou: Scr. Mater. 65 (2011) 281–284. DOI:10.1016/j.scriptamat.2011.04.023
[23] H.Q. Hao, W.G. Jiang, G. Xie, G. Zhang, Y.Z. Lu, J. Zhang, L.H. Lou: Prog. Nat. Sci. 23 (2013) 211–215. DOI:10.1016/j.pnsc.2013.03.007
[24] G.W. Wang, J.J. Liang, Y.Z. Zhou, T. Jin, X.F. Sun, Z.Q. Hu: J. Mater. Sci. Technol. (2016) in press. DOI:10.1016/j.jmst.2016.05.007
[25] X.L. Yang, H.B. Dong, W. Wang, P.D. Lee: Mater. Sci. Eng. A 396 (2004) 129–139. DOI:10.1016/j.msea.2004.07.007
[26] R.E. Napolitano, R.J. Schaefer: J. Mater. Sci. 35 (2000) 1641–1659. DOI:10.1023/A:1004747612160
[27] X.J. Yan, Y. Deng, R.J. Sun, J.W. Xie: Acta Aeronaut. Astronaut. Sinica 32 (2011) 1930–1936.
[28] A. Bussac, C.A. Gandin: Mater. Sci. Eng. A 237 (1997) 35–42. DOI:10.1016/S0921-5093(97)00081-6
[29] Z.X. Shi, J.R. Li, S.Z. Liu, J.Q. Zhao: J. Aeronaut. Mater. 29 (2009) 88–92.
[30] Z.X. Shi, J.R. Li, S.Z. Liu, J.Q. Zhao: Rare Met. Mater. Eng. 41 (2012) 962–966. DOI:10.1016/S1875–5372(12)60053–8
[31] M. Huang, L.C. Zhuo, Z.L. Liu, X.G. Lu, Z.X. Shi, J.R. Li, J. Zhu: Mater. Sci. Eng. A 640 (2015) 394–401. DOI:10.1016/j.msea.2015.05.089
[32] Q.Z. Chen, C.N. Jones, D.M. Knowes: Mater. Sci. Eng. A 385 (2004) 402–418. DOI:10.1016/j.msea.2004.07.013
[33] X.B. Zhao, L. Liu, W.G. Zhang, M. Qu, J. Zhang, H.Z. Fu: Rare Met. Mater. Eng. 40 (2011) 9–13. DOI:10.1016/S1875–5372(11)60009-X
[34] Z.X. Shi, S.Z. Liu, J.R. Li: Foundry 64 (2015) 153–156.
[35] C.L. Dong, H.C. Yu, Y. Li, X.G. Yang, D.Q. Shi: Int. J. Fatigue 61 (2014) 21–27. DOI:10.1016/j.ijfatigue.2013.11.026
[36] C.L. Dong, H.C. Yu, Y. Li: Mater. Des. 66 (2015) 284–293. DOI:10.1016/j.matdes.2014.10.071
[37] Z.X. Wen, H.Q. Pei, B.Z. Wang, D.X. Zhang, Z.F.Yue: Mater. High Temp. 33 (2016) 68–74. DOI:10.1080/09603409.2015.1106786
[38] B.Z. Wang, D.S. Liu, Z.X. Wen, Z.F. Yue: Mater. Sci. Eng. A 593 (2014) 31–37. DOI:10.1016/j.msea.2013.09.013
[39] D. Leidermark, J.J. Moverare, S. Johansson, K. Simonsson, S. Sjostrom: Acta Mater. 58 (2010) 4986–4997. DOI:10.1016/j.actamat.2010.05.032
[40] Q. Qin, J.L. Bassani: J. Mech. Phys. Solids 40 (1992) 813–833. DOI:10.1016/0022-5096(92)90005-M
[41] D. Leidermark, J. Moverare, K. Simonsson, S. Sjostrom, S. Johansson: Comp. Mater. Sci. 47 (2009) 366–372. DOI:10.1016/j.commatsci.2009.08.012

[42] Q. Qin, J.L. Bassani: J. Mech. Phys. Solids 40 (1992) 835–862. DOI:10.1016/0022-5096(92)90006-N
[43] J.L. Chaboche: Int. J. Plast. 5 (1989) 247–302. DOI:10.1016/0749-6419(89)90015-6
[44] F. Shi: Re-development of ANSYS and application examples, China Water & Power Press, Beijing (2012).
[45] J.W. Park, S.S. Babu, J.M. Vitek, E.A. Kenik, S.A. David: J. Appl. Phys. 94 (2003) 4203–4209. DOI:10.1063/1.1602950
[46] J.M. Vitek: Acta Mater. 53 (2005) 53–67. DOI:10.1016/j.actamat.2004.08.039

(Received October 24, 2016; accepted December 12, 2016; online since January 27, 2017)

Correspondence address

Haibin Tang, Ph.D.
College of Energy and Power Engineering
Nanjing University of Aeronautics and Astronautics
29 Yudao Street
Nanjing 210016
China
Tel.: +86-15151865950
E-mail: haibint@umich.edu

Bibliography
DOI 10.3139/146.111466
Int. J. Mater. Res. (formerly Z. Metallkd.)
108 (2017) 3; page 163–172

ISSN 1862-5282